

Commensurate-incommensurate transition of monolayer krypton on graphite by helium-atom scattering

S. Chung, A. Kara, J. Z. Larese,* W. Y. Leung,[†] and D. R. Frankl

Department of Physics, The Pennsylvania State University, University Park, Pennsylvania 16802

(Received 23 May 1986; revised manuscript received 13 November 1986)

The commensurate-incommensurate transition of monolayer krypton films on a graphite single-crystal substrate is observed by helium-atom diffraction for transition temperatures in the range 50–60 K. The change in lattice spacing appears continuous, with an upper limit of 0.3% on a possible jump, with no detectable hysteresis. The slightly incommensurate phase is disordered but apparently well correlated. The spatial correlation length changes in a possibly discontinuous manner. A decrease of specular and diffracted intensities while the film is still commensurate is observed. This may be due to incoherent elastic scattering from isolated defects, or possibly to increased inelastic scattering.

INTRODUCTION

The krypton monolayer physisorbed on the graphite basal plane has been extensively investigated over the past half-dozen years because it exemplifies the interesting behavior that can occur in the presence of two competing spatial periodicities. The natural Kr-Kr interatomic distance is a few percent smaller than the spacing of second-neighbor graphite cells, but the corrugation of the Kr-graphite potential is sufficiently strong that the Kr atoms can be held in these cells to form a commensurate (C) monolayer. This may, however, undergo a phase transition to a more dense incommensurate (IC) layer which exists over an appreciable temperature and pressure range before second-layer condensation sets in.

The commensurate-incommensurate transition (CIT) was first discovered in volumetric adsorption measurements^{1,2} in the range of about 70–125 K and 10^{-3} to 500 Torr. It was also found by electron diffraction^{3,4} to occur in the (50–60)-K, (10^{-8} – 10^{-6})-Torr range, and, by x-ray diffraction,⁵ in the (80–90)-K, (10^{-2} –1)-Torr range. The diffraction results generally indicated a continuous variation of lattice constant, such that the incommensurability $\delta\epsilon$ [shift in reciprocal-lattice constant (τ) from the commensurate value (τ_c), i.e., $\delta\epsilon = \tau - \tau_c$] behaved approximately as

$$\delta\epsilon = \epsilon_0 \left[1 - \frac{T}{T_c(p)} \right]^{1/3}. \quad (1)$$

One exception was the work of Bohr *et al.*,⁶ which indicated a first-order transition, showing coexistence of C and IC phases; however, in this study the CIT was driven by D_2 spreading pressure.

The high-resolution synchrotron x-ray-scattering results of Moncton *et al.*⁷ emphasized the presence of strong disorder when the film was only slightly incommensurate, i.e., at temperatures just slightly below T_c . The authors described this as a “liquidlike” phase. Indeed, later studies in the (115–130)-K, (100–600)-Torr range⁸ reported that a truly fluid phase (the “reentrant fluid”) intervenes

between the C and IC solid phases. A detailed study of the transition was also carried out by Stephens *et al.*⁹ in the (90–100)-K range. They, too, found a decrease and broadening of the diffracted peak. Apparent coexistence of a C and a slightly IC phase in two of the three runs was attributed to a “distribution of critical points” which may have been the result of the particular form of graphite substrate (ZYX) they used.

Another intriguing aspect of the transition is the rotation of the IC phase relative to the graphite lattice. This was first predicted by Novaco and McTague¹⁰ and verified by means of low-energy electron diffraction¹¹ (LEED) and transmission high-energy electron-diffraction THEED (Ref. 4) measurements. Shiba¹² calculated the variation of rotation angle with degree of misfit, and this too was verified by means of synchrotron x-ray diffraction.¹³

The present paper describes a study of this transition by means of helium-atom scattering. Though inherently of lower resolving power than synchrotron x rays, this probe offers certain unique advantages in the complete absence of penetration, in the availability of information in the specular as well as the diffracted beams, and in the sensitivity to surface defects.

EXPERIMENTAL METHODS

The apparatus has been described before.¹⁴ In brief, it is comprised of a cryopumped ultrahigh-vacuum (UHV) chamber equipped with a cooled two-axis sample goniometer, a movable quadrupole-mass-spectrometer detector, LEED-Auger optics, and a supersonic helium-atom beam source. In the latter, ^4He gas is expanded from about 50 bars at 77 K through a 5 μm nozzle followed by two differential pumping stages. The beam-velocity spread is less than 1% full width at half maximum (FWHM). The mean wavelength, as determined by diffraction from bare graphite samples, is observed to vary slightly from day to day as the liquid-nitrogen coolant ages. The angular divergence is 0.03° (full angle) and the beam width at the crystal is about 0.4 mm. The detector aperture swings on a 50-mm arc and just accepts the full beam, so the FWHM of the direct-beam signal is slightly under 0.3°.

The beam source is flexibly coupled to the scattering chamber, so that it may be moved laterally to search for a nearly flat area of the crystal sample.

The substrate samples used for these experiments are flakes of natural graphite single crystals that were extracted from a Ticonderoga, NY, ore kindly supplied by Dr. T. S. Noggle of Oak Ridge National Laboratory. They are approximately 2–4 mm in diameter and 0.5 mm thick, selected for flatness by optical microscopy and laser-beam reflection. The selected crystal is mounted with epoxy onto a spring-loaded oxygen-free high-conductivity copper rocker plate for adjustment of position and tilt. Final small trimming adjustments can be made *in situ* under vacuum by means of a bellows-mounted screwdriver. The copper rocker plate is mounted on the two-axis goniometer and is thermally linked by copper braids to a Displex (Air Products Co.) closed-cycle refrigerator. The crystal is cleaved in air using transparent adhesive tape. A base pressure of 2×10^{-10} Torr is typically obtained after a 24-h bakeout at 120°C. Prior to each experimental run the crystal is heated by electron bombardment from behind the rocker plate to about 700 K for about 1 h. After cooling, the temperature of the crystal mounting plate, as measured by a platinum-resistance thermometer, has long-term stability of about ± 0.1 K.

Krypton films were grown by cooling the graphite crystal to 50–60 K and admitting research-grade krypton gas (99.995%) through a UHV leak valve via a stainless-steel capillary which was aimed either at the crystal (direct dosing) or at the wall of the vacuum chamber (indirect dosing). In either case, the specular beam intensity was monitored continuously during the deposition. Typically, the specular reflection intensity decreases quite linearly with time in the beginning of the deposition, then levels off to a final steady value. A nude ionization gauge, not separately calibrated for Kr, measures the background pressure in the chamber. In the case of direct dosing, the static background pressure rises during the deposition by about $(2-5) \times 10^{-10}$ Torr depending on the valve opening. A simple calculation shows that the effective pressure of the Kr gas at the crystal surface is roughly 10^2 times higher.¹⁴ For indirect dosing, higher chamber pressures were used.

The incident beam is chopped mechanically in the second stage of the source at a frequency of about 200 Hz with a 40% duty cycle, and the detector output is measured in analog form on a lock-in amplifier. For the most painstaking measurements of diffracted beams, the detector was moved in increments of 0.05°, the lock-in time constant was set at 4 sec, and the signal recorded after a lapse of 12 sec. A 5° scan through a peak thus took about 20 min. In cases where the temperature was varied, a period of up to 30 min was allowed for stabilization before starting each scan, whereas a 15-min interval was used for the constant-pressure runs.

EXPERIMENTAL RESULTS

Dosing

The general behavior on admission of the Kr has been described.¹⁵ In brief, the specular intensity decreases

markedly then levels off, the bare graphite selective adsorption pattern disappears, and the $(\bar{1},0)$ diffraction peak from a $\sqrt{3} \times \sqrt{3} R 30^\circ$ structure appears and grows. Under suitable conditions of temperature and dose rate, the position of this peak corresponds exactly (within $\pm 1\%$) to the commensurate spacing ($Q=1.70 \text{ \AA}^{-1}$). In a few cases, a break in the slope of the specular intensity decrease, similar to that found on close-packed metal surfaces,¹⁶ was observed, but a complete characterization of this behavior has not yet been carried out. Furthermore, the exact conditions leading to a commensurate monolayer are still not completely known. Slow dosing, i.e., a deposition time of about 20 min, has generally proved successful. Higher krypton pressures or lower crystal temperatures (e.g., < 50 K) usually resulted in IC films. These could, however, be driven into the C phase by gentle annealing.

Diffraction

Figure 1 gives examples of the $(0,0)$ and $(\bar{1},0)$ peaks from the Kr overlayer, with a 17-meV beam incident at 70° in the $(1,0)$ azimuth. The complex shape of the $(0,0)$ beam indicates that at least two major facets of the crystal are contributing to the reflection. However, the leading edge of the stronger peak, up to and somewhat beyond the maximum, looks like a sharp single reflection. Accordingly, we take the first half of this peak, along with its

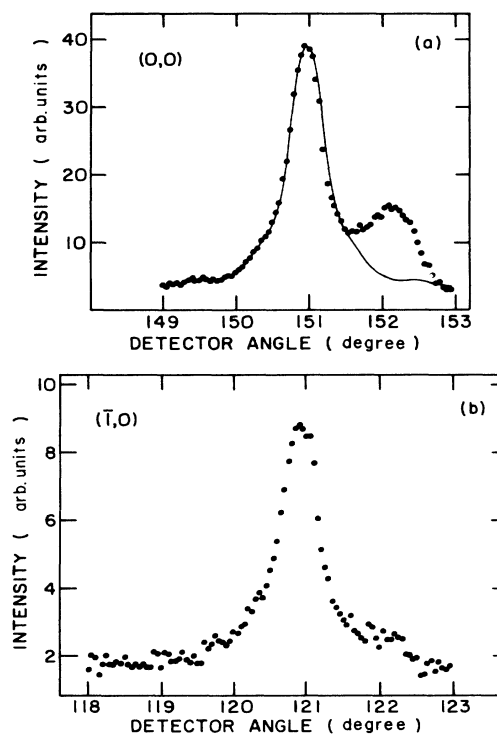


FIG. 1. Polar scans of He diffraction from the commensurate Kr monolayer on graphite with $E_i=17$ meV at $\sigma_c=70.4$. (a) $(0,0)$ peak, solid line is the smoothed and symmetrized one; (b) $(\bar{1},0)$ peak.

mirror image, to represent the measured single-facet reflection. The shape, after smoothing the data by a weighted spline-fitting algorithm, is also shown in Fig. 1(a). The width of this peak represents the overall broadening due to imperfect collimation, finite detector-aperture width, and aplanarity of the principal facet. Broadening due to the wavelength spread of the beam is, of course, not included in the specular beam; however, diffraction from bare graphite and other crystals in the past has shown this to be negligible relative to the other sources of broadening. We have therefore taken the solid curve of Fig. 1(a) to represent the fully-instrument-broadened line. It can be well fitted by a Lorentzian atop a constant background. We designate this "instrument response function" as $B(Q)$, where $Q = 2k_i \sin \theta$.

The measured diffraction peak $I^m(Q)$ of Fig. 1(b) is the convolution of a "true" diffraction peak $I(Q)$ with the instrument response function

$$I^m(Q) = I(Q) * B(Q). \quad (2)$$

Deconvolution of the experimental data was performed in the following way. The raw diffraction data was initially smoothed and symmetrized in order to first extract the peak position, τ . A parametrized functional form for $I(Q)$ was convoluted with the previously determined instrument function and then least-squares-fitted to $I^m(Q)$. A simple empirical functional form which describes the data well is

$$I(Q) = \frac{A\sigma^2}{(Q - \tau)^2 + \sigma^2}. \quad (3)$$

The amplitude A and the linewidth σ were treated as free parameters in the fitting procedure. A typical example of the fit to the raw data is illustrated in Fig. 2. Although the secondary crystal facets are much less prominent in the diffraction data [compare, e.g., Figs. 1(a) and 1(b) at larger detector angles], the fitting procedure was applied *only* to the first half of the peak. The reduced prominence is presumably due to the azimuthal misalignment of the minor facet.

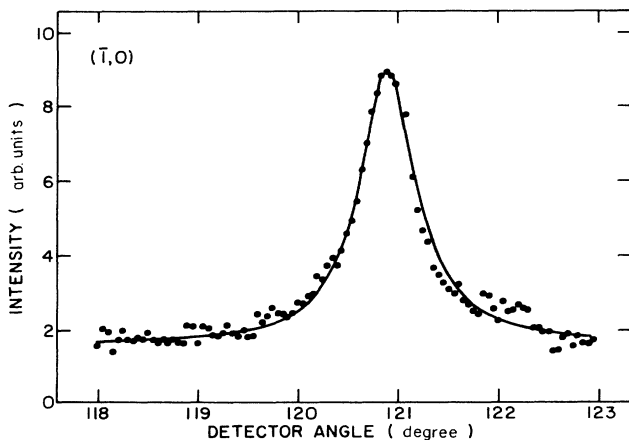


FIG. 2. Same as in Fig. 1. $(\bar{1},0)$ diffraction peak. Solid line is the fit as discussed in the text.

A summary of the fitted parameters is shown in Fig. 3 for two constant-pressure runs as the substrate temperature was incrementally decreased. In Fig. 3(a) the peak position τ is found to be nearly constant at the C position of 1.70 \AA^{-1} until the temperature reaches 51.0 K, at which point an abrupt increase begins. The change in τ , however, appears continuous, with 0.3% as an upper limit to a first-order jump. No detectible evidence for two-phase coexistence appears in this region. In the neighborhood of the transition the incommensurability follows Eq. (1), as shown by the solid line. Far from the transition the misfit saturates at a $\tau \approx 1.79 \text{ \AA}^{-1}$, characterizing the "fully IC" phase.

Figure 3(b) illustrates the half-width behavior of the data. This, too, is remarkably constant throughout the C range, where its value of 0.0018 \AA^{-1} indicates that a spatial correlation length (π/σ) of about 1700 \AA is characteristic of the C phase. The coherent domain size of the graphite substrate is at least comparably large, as indicated by diffraction-line widths. At the transition, σ increases abruptly (by approximately threefold), rises rapidly to a maximum of 0.006 \AA^{-1} ($\pi/\sigma \approx 500 \text{ \AA}$), and then steadily decreases with decreasing temperature. Although the absolute values of the coherence lengths are somewhat uncertain owing to the necessity of deconvolution, the marked changes, which are evident directly in the raw data, are the important points here. This marked line broadening for the weakly incommensurate phase is indicative of a significant amount of disorder associated with this density regime. The ratio ϵ/σ is plotted versus ϵ in Fig. 4.

The integrated intensities of the $(0,0)$ and $(\bar{1},0)$ peaks

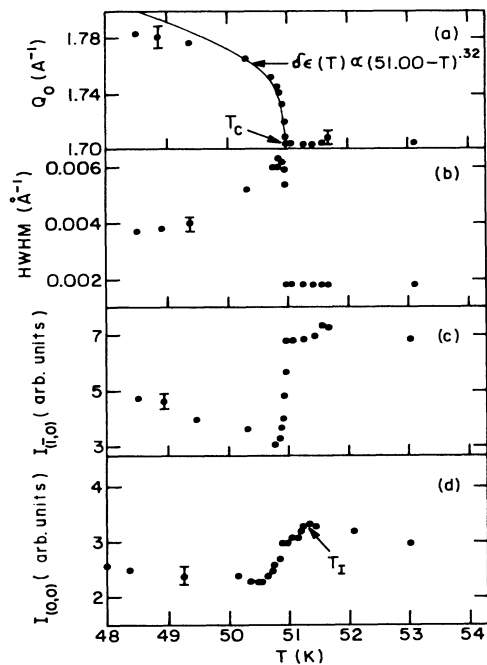


FIG. 3. Parameters for two constant-pressure runs; (d) was obtained in a separate run. Solid line is a least-squares fit to a power law: $\delta\epsilon(T) = 0.07425(51.00 - T)^{0.32}$.

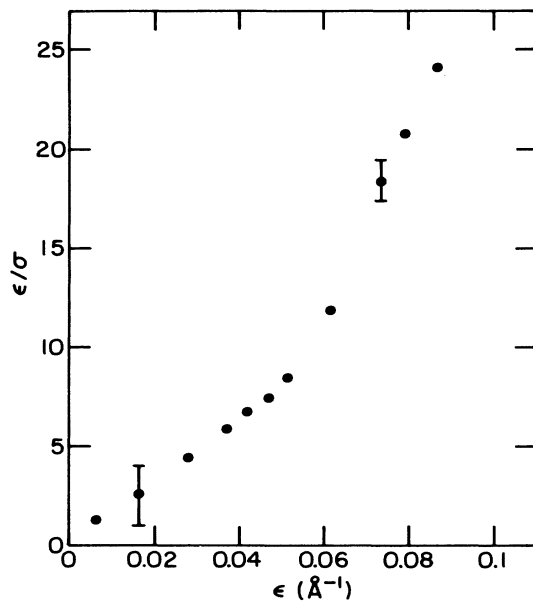


FIG. 4. Ratio of peak shift to peak width as a function of peak shift. Compare with Fig. 13 of Stephens *et al.* (Ref. 9).

are shown in Figs. 3(c) and 3(d), respectively. At temperatures well above T_c , the intensities increase with decreasing temperature according to the Debye-Waller effect. But at a temperature T_I about 0.5 K above T_c they begin to decrease. At T_c , there is an abrupt intensity decrease accompanying the broadening.

Thereafter, both intensities come to minima and slowly increase. In several other constant-pressure runs at higher Kr pressures (giving higher T_c values), the initial intensity decrease at T_I was much less pronounced, disappearing at $T_c = 57.5$ K. Attempts were also made to follow the effects to lower T_c , but owing to poor controllability of the leak valve the film always turned out to be IC as-deposited, and the transition to the C phase upon warming was never found below 50.5 K.

Several runs were made in both directions through the transition. An example is shown in Fig. 5. The measured τ values are quite closely reproduced upon both heating and cooling, so that there is no pronounced hysteresis evident. The small discrepancies might be due to imperfect thermal equilibration.

Numerous earlier runs were made by increasing the Kr pressure at constant temperature. The results are shown in Fig. 6. Again, using the peak positions to indicate the incommensurability, the near-transition region is described fairly well by

$$\delta\epsilon = \epsilon_0 \left[\frac{p'}{p'_c(T)} - 1 \right]^{1/3}, \quad (4)$$

where p' is the pressure rise in the scattering chamber due to the influx of the Kr gas, and p'_c is the value of the latter at the onset of the transition. The relation of p'_c to T is shown in Fig. 7. The points determined by direct dosing fall into two sets differing by about tenfold in pressure. Since the dosing tube was moved several times and was

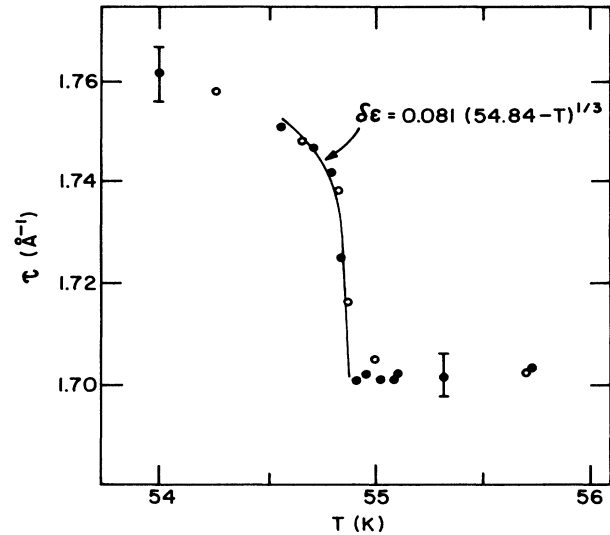


FIG. 5. Temperature dependence of $(\bar{1},0)$ peak position. Solid circle, decreasing temperature; open circle, increasing temperature. Solid line is a least-squares fit to Eq. (1).

not very precisely fixed in position, the difference is probably attributable to changes in flow geometry. Both sets have about the same slope as the data of Ref. 3, which were measured under static conditions with a calibrated gauge. Our attempt to approximate static conditions by indirect dosing (gas inlet tube aimed away from the crystal) gave rather erratic results which lie about one decade in pressure below those of Ref. 3.

A few azimuthal scans were made to investigate the rotation of the IC phase. The results were generally consistent with previous LEED measurements³ performed in the same temperature range, but we shall not discuss them in detail here.

DISCUSSION

A number of conclusions from this study confirm and/or extend those of previous work.

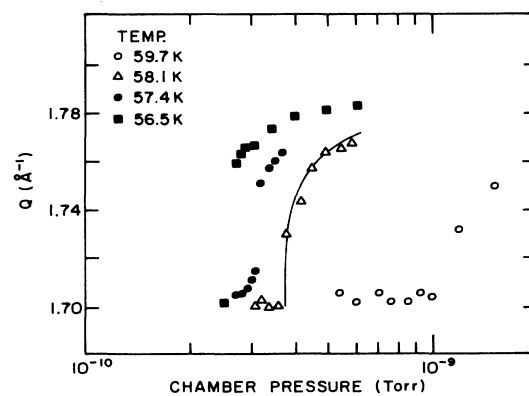


FIG. 6. $(\bar{1},0)$ peak position at different crystal temperatures while changing the chamber pressure. Solid line is a least-squares fit to Eq. (4).

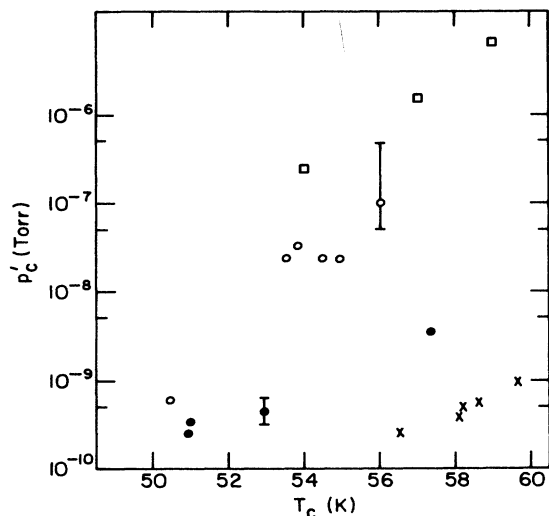


FIG. 7. The critical chamber pressure vs temperature at C-IC transition. Solid and open circles show direct and indirect dosing, respectively, for constant-pressure runs. Crosses show direct dosing for constant-temperature runs from Fig. 6. Squares show LEED results, Refs. 3.

(1) The lattice-spacing transition is a continuous one, as indicated by the absence of significant discontinuity ($<0.3\%$), hysteresis, or two-phase coexistence. This conclusion agrees with those of the previous x-ray studies, all of which were at a higher temperature. In the two x-ray runs on one sample where apparent coexistence was observed,⁹ it was attributed by its authors to a "distribution of critical points." Earlier LEED (Ref. 3) and THEED (Ref. 4) studies in the lower-temperature range also indicated continuity.

(2) The incommensurability follows the $\frac{1}{3}$ -power law of Eq. (19) near the transition, again in agreement with earlier work (e.g., Fig. 1 of Ref. 9). We observe a saturation at about 5% linear compression, as would be expected from the size of the krypton atoms.

(3) An uncharacterized disordered phase (referred to in earlier works as a "reentrant fluid") intervenes between the highly ordered C phase and the fairly well-ordered fully IC phase. This has been one of the main points of interest since its discovery at higher temperatures by x-ray diffraction.⁷ Indeed, at high temperatures, the disorder is so great that the phase has been designated a fluid. In the present work, the disorder never reaches this extreme, and the film appears reasonably well correlated throughout the transition.

(4) The range of spatial correlations (π/σ) of the film changes in a seemingly *discontinuous* manner at the transition. Starting from the rather large value of nearly 2000 Å in the C phase, there is an abrupt change, by nearly a factor of 3, with barely any shift of the diffraction peak.

Perhaps the increased linewidth and decrease in peak intensity are related to the formation of unresolved weak superlattice peaks^{5,7} associated with domain-wall formation. The exact values of the correlation length depend, of course, on the exact functional form for the line shape used in the deconvolution procedure, but the trend is unmistakable even in the raw data. The x-ray data show much more gradual changes, possibly owing to the much better instrumental resolution.

(5) In agreement with x-ray results, the range of spatial correlations again increase as the fully-IC state is approached. The size seems to level off at about half the C-phase size, which may be associated with the presence of two oppositely rotated domains.

(6) The ratio ϵ/σ , shown in Fig. 5, may behave somewhat differently than in the x-ray data (Fig. 13 of Ref. 9). The trend seems to indicate $\epsilon/\sigma \propto \epsilon$ for small values. This, of course, simply reflects the relatively slow variation of σ once $T < T_c$. However, the relative-error limits on the small values of ϵ are so great that the limiting behavior $\epsilon/\sigma \rightarrow 1$ cannot be totally ruled out.

The foregoing features tend, broadly speaking, to confirm the main conclusions of the x-ray experiments and to extend them to lower temperature. The intervening disordered phase is, however, not as highly disordered at the lower temperature, so the nature of the transition may be somewhat different in detail. One possible scenario is the formation of isolated localized defects that would act as random uncorrelated scattering centers without shifting the diffraction-line position. These defects might be isolated single atoms or small clusters in the second layer, or interstitials in the first layer. In either case, one could speculate that their formation could act as a precursor to the transition in that the accumulation of a sufficient number could trigger their condensation into the domain walls usually invoked to describe the main transition. An alternative possibility is an increase in the inelastic background scattering due to the softening of one or more phonon modes.

Clearly, it will be of interest to extend these observations to still lower temperatures and more fully characterize the rotation of the IC domains (our preliminary azimuthal scans of the diffraction peaks are generally consistent with the LEED and x-ray results). Our further attempts to do so have thus far been frustrated by lack of precise pressure control and understanding of the condensation kinetics. We plan to pursue these matters in the near future.

ACKNOWLEDGMENTS

We are grateful to Professor M. W. Cole for extensive and stimulating discussions, to Professor J. Pliva for much help with the computations, and to Professor J. R. Manson for helpful discussions. The work was supported by the National Science Foundation under Grant No. DMR-84-19261.

- *Present address: Physics Department, Brookhaven National Laboratory, Upton NY 11973.
- †Present address: Physics Department, Iowa State University, Ames, IA 50011.
- ¹A. Thomy and X. Duval, *J. Chim. Phys.* **67**, 1101 (1970).
- ²Y. Larher, *J. Chem. Phys.* **68**, 2257 (1978).
- ³M. D. Chinn and S. C. Fain, Jr., *Phys. Rev. Lett.* **39**, 146 (1977); S. C. Fain, M. D. Chinn, and R. D. Diehl, *Phys. Rev. B* **21**, 4170 (1980).
- ⁴P. S. Schabes-Retchkiman and J. A. Venables, *Surf. Sci.* **105**, 536 (1981).
- ⁵P. W. Stephens, P. Heiney, R. J. Birgeneau, and P. M. Horn, *Phys. Rev. Lett.* **43**, 47 (1979).
- ⁶J. Bohr, M. Nielsen, and J. Als-Nielsen, in *Proceedings of the 3rd European Conference on Surface Science (Paris, 1980)*, p. 1533 (unpublished).
- ⁷D. E. Moncton, P. W. Stephens, R. J. Birgeneau, P. M. Horn, and G. S. Brown, *Phys. Rev. Lett.* **46**, 1533 (1981).
- ⁸E. D. Specht, M. Sutton, R. J. Birgeneau, D. E. Moncton, and P. M. Horn, *Phys. Rev. B* **30**, 1589 (1984).
- ⁹P. W. Stephens, P. A. Heiney, R. J. Birgeneau, P. M. Horn, D. E. Moncton, and G. S. Brown, *Phys. Rev. B* **29**, 3512 (1984).
- ¹⁰A. D. Novaco and J. P. McTague, *Phys. Rev. Lett.* **38**, 1286 (1977); J. P. McTague and A. D. Novaco, *Phys. Rev. B* **19**, 5299 (1977).
- ¹¹S. C. Fain, Jr., M. D. Chinn, and R. D. Diehl, *Phys. Rev. B* **21**, 4170 (1980).
- ¹²H. Shiba, *J. Phys. Soc. Jpn.* **48**, 211 (1980).
- ¹³K. L. D'Amico, D. E. Moncton, E. D. Specht, R. J. Birgeneau, S. E. Nagler, and P. M. Horn, *Phys. Rev. Lett.* **53**, 2250 (1984).
- ¹⁴W. Y. Leung, Ph.D. thesis, The Pennsylvania State University, 1985 (unpublished).
- ¹⁵J. Z. Larese, W. Y. Leung, D. R. Frankl, N. Holter, S. Chung, and M. W. Cole, *Phys. Rev. Lett.* **54**, 2533 (1985).
- ¹⁶B. Poelsema, L. K. Verheij, and G. Comsa, *Phys. Rev. Lett.* **51**, 2410 (1983).